Inorganic Chemistry

Article

pubs.acs.org/IC

Complex Cation Order in Anion-Deficient $Ba_nYFe_{n-1}O_{2.5n}$ Perovskite Phases

Kun Luo and Michael A. Hayward*

Department of Chemistry, University of Oxford, Inorganic Chemistry Laboratory, South Parks Road, Oxford, OX1 3QR, United Kingdom

ABSTRACT: The synthesis and structural characterization of $Ba_nYFe_{n-1}O_{2.5n}$ (n = 2, 3, 4) anion-deficient perovskite phases is reported. The n = 2 and n = 3 members of the series, Ba_2YFeO_5 and $Ba_3YFe_2O_{7.5}$, adopt structures which consist of ordered arrays of corner-linked YO_6 octahedra and FeO_4 tetrahedra on the perovskite B-sites and are described in unit cells related to a simple cubic perovskite cell by respective $2\sqrt{2} \times \sqrt{2} \times 2$ and $3\sqrt{2} \times \sqrt{2} \times 2$ geometric expansions. The complex cation ordering schemes observed in the two phases can be described on the basis of $Y_2Fe_2O_{10}\square_2$ secondary building units. A rationalization for the observed structures is presented on the basis of the need to minimize lattice strain while maintaining the integrity of the local YO_6 and FeO_4 coordination polyhedra. The n = 4 member of the series, $Ba_4YFe_3O_{10}$, adopts a cation and anion-vacancy disordered structure, which is attributed to dilution of the structure directing effects at extreme Y:Fe stoichiometric ratios. Magnetization data indicate Ba_2YFeO_5 and $Ba_3YFe_2O_{7.5}$ exhibit paramagnetic behavior, consistent with the lack of a long-range Fe−O−Fe network. $Ba_4YFe_3O_{10}$ adopts an antiferromagnetic state below 50 K.

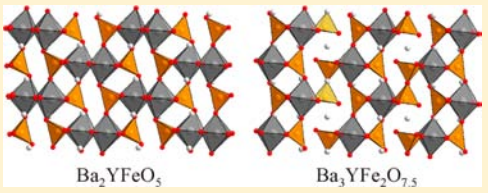

INTRODUCTION

Complex transition metal oxide phases based on the ABO_3 cubic perovskite structure have been the subject of intense and sustained study due to the wide variety of academically interesting and industrially applicable properties they exhibit.[1] Accompanying these diverse physical properties is a flexible and adaptable chemistry which allows a wide variety of cations to be accommodated within the extended lattice and which tolerates a broad range of oxygen nonstoichiometry. As a result perovskite phases offer chemists a huge number of opportunities to prepare new materials and modify the behavior of existing phases through elemental substitution.

A class of phases which has been receiving particular attention recently are the cation ordered perovskites.[2,3] These are materials which have ordered arrays of two or more cations on the A- and/or B-sites of the extended perovskite framework, with the simplest examples having formulas such as $AA'B_2O_6$ and $A_2BB'O_6$. Interest in these materials stems from the observation that cation ordered materials often exhibit physical behavior which is significantly different from that of the analogous cation disordered materials. For example the cation ordered phase Sr_2FeMoO_6 exhibits magnetoresistive behavior,[4] and A-cation ordered phase $LaBaMn_2O_6$ has a different ferromagnetic ordering temperature to the analogous A-cation disordered phase $La_{0.5}Ba_{0.5}MnO_3$.[5]

However, despite the interest in cation ordered perovskites phases, the preparation of materials which exhibit complex cation order is a long-standing challenge in solid state synthesis. Principally this is because at the high temperatures required for the synthesis of complex oxide phases, entropy plays a dominant role in thermodynamic equilibrium between different competing structure types and cation arrangements, strongly favoring materials with statistically disordered cation arrangements. Therefore, in order to overcome this entropically driven preference for disorder, a strong enthalpic motivation to form ordered phases must be provided.

Conventionally, cation order is induced into perovskite phases and other suitable host lattices by utilizing cations which are dissimilar in charge and/or size. Ordered structures tend to be favored under these circumstances because they have better local charge neutrality and lower lattice strain compared to disordered structures. However this strategy is rather limited because the cations being ordered must have a large difference in size and/or charge, a rather onerous restriction, and the ordered phases prepared tend to adopt rather simple ordering patterns such as the rock salt, columnar, or layered arrangements shown in Figure 1a.[2,3]

In order to extend both the variety of cations that can be ordered and the complexity of the ordering patterns formed, we and others have recently been utilizing a different strategy to prepare cation ordered perovskite phases.[6−8] This makes use of the observation that some cations strongly favor particular coordination numbers and geometries due to their size and/or d-electron count. By introducing large levels of anion deficiency into the host perovskite lattice, the differing coordination preferences of cations can be utilized to bring about a synergic ordering of both cations and anion-vacancies to yield novel phases with complex cation ordered lattices.

By following this strategy we were able to prepare the complex cation ordered perovskite phase $Ba_4CaFe_3O_{9.5}$ in which the differing coordination preferences of Ca^{2+} and Fe^{3+} interact with the anion deficiency of the material to form a highly complex cation ordered structure (Figure 1b), which lifts

Received: July 18, 2012
Published: November 1, 2012

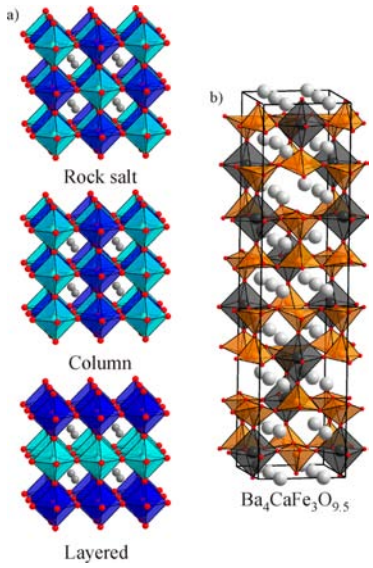

Figure 1. (a) Common B-site cation ordering schemes: rock salt, column, and layered. (b) The complex cation ordered strucutre of $Ba_4CaFe_3O_{9.5}$.

the inversion symmetry of the host perovskite lattice to yield an acentric phase which exhibits second harmonic generation.[8]

Building on this work we have prepared a series of $Ba_nYFe_{n-1}O_{2.5n}$ perovskite phases which adopt complex cation-ordered structures via an analogous simultaneous ordering of cations and anion vacancies.

EXPERIMENTAL SECTION

Synthesis. Samples of composition $Ba_nYFe_{n-1}O_{2.5n}$ (n = 2, 3, 4) were prepared via a high-temperature ceramic synthesis route. Suitable stoichiometric ratios of $BaCO_3$ (99.997%), Y_2O_3 (99.998%, dried at 900 °C), and Fe_2O_3 (99.99%) were ground together in an agate pestle and mortar and then heated in air at 1000 °C to decompose the carbonate. The resulting material was then reground, pressed into 13 mm pellets, and heated at 1425 °C for two periods of 40 h under flowing argon.

Characterization. X-ray powder diffraction data were collected using a PANalytical X'pert diffractometer incorporating an X'celerator position-sensitive detector (monochromatic Cu Kα1 radiation). Neutron powder diffraction data were collected using the D2b diffractometer (λ = 1.59 Å) at the ILL neutron source in Grenoble, France, and the POLARIS diffractometer at the ISIS neutron source, U.K. Rietveld profile refinements were performed using the GSAS suite of programs.[9] Average iron oxidation states in all phases were determined by iodometric titration. Samples were dissolved in a dilute HCl solution containing an excess of KI, and the liberated I_2 was titrated with $Na_2S_2O_3$ solution. Magnetization data were collected using a Quantum Design MPMS SQUID magnetometer.

RESULTS

Iodometric titrations performed on all $Ba_nYFe_{n-1}O_{2.5n}$ (n = 2, 3, 4) samples were consistent with an average iron oxidation state of Fe^{3+}, confirming the stated compositions.

Structural Characterization of Ba_2YFeO_5. X-ray and neutron powder diffraction data collected from Ba_2YFeO_5 could be readily indexed using a monoclinic unit cell [a = 12.5860(1) Å, b = 6.08289(7) Å, c = 7.8070(1) Å, β = 92.247(1)°, V = 597.24(3) Å^3] with extinction conditions consistent with $P2_1/n$ space group symmetry. In order to determine the structure of Ba_2YFeO_5, a series of structural models based on known cation-ordered $Ba_2MM'O_5$ phases were prepared and compared to the diffraction data. A model based on the structure of Ba_2NdAlO_5[10] was observed to account for the majority of the observed diffraction features well, when neodymium was replaced by yttrium and aluminum replaced by iron, suggesting Ba_2NdAlO_5 and Ba_2YFeO_5 share a common cation-ordered structure. However, the unit cell reported for Ba_2NdAlO_5 [a = 7.314(2) Å, b = 6.120(1) Å, c = 7.525(2) Å, β = 117.64(2)°, V = 298.3(31) Å^3] has only half the volume of the smallest cell required to index the diffraction data collected from Ba_2YFeO_5. Therefore, an adapted structural model based on the cation-ordered structure of Ba_2NdAlO_5 was constructed in the larger cell determined from the Ba_2YFeO_5 diffraction data, consistent with $P2_1/n$ space group symmetry. Refinement of this expanded model against neutron powder diffraction data collected from Ba_2YFeO_5 converged rapidly to give a good statistical fit (χ^2 = 2.81). Refinement of the yttrium and iron site occupancies revealed no evidence of antisite cation disorder. Full details of the refined structure of Ba_2YFeO_5 are given in Table 1, with selected bond lengths in Table 2.

Table 1. Refined Structural Parameters of Ba_2YFeO_5[a]

atom	site	x	y	z	U_{iso} (Å^2)
Ba(1)	4e	0.1529(2)	0.2585(10)	0.0176(4)	0.0073(8)
Ba(2)	4e	0.1168(2)	0.2559(9)	0.5087(4)	0.0032(7)
Y(1)	4e	0.8697(2)	0.2497(8)	0.2297(3)	0.0035(5)
Fe(1)	4e	0.9157(1)	0.2369(4)	0.7570(2)	0.0017(4)
O(1)	4e	0.8710(2)	0.2598(7)	0.5252(4)	0.0087(7)
O(2)	4e	0.3194(2)	0.2377(9)	0.4319(4)	0.0101(8)
O(3)	4e	0.2285(3)	0.0445(7)	0.7530(5)	0.0064(8)
O(4)	4e	0.5201(3)	0.0409(6)	0.2829(4)	0.0071(8)
O(5)	4e	0.4822(3)	0.5381(7)	0.2707(5)	0.0097(9)

[a] Ba_2YFeO_5: space group $P2_1/n$, a = 12.5860(1) Å, b = 6.08289(7) Å, c = 7.8070(1) Å, β = 92.247(1)°, χ^2 = 2.81, wRp = 4.11%, Rp = 3.18%.

Table 2. Selected Bond Lengths from the Refined Structure of Ba_2YFeO_5

cation	anion	bond length (Å)	BVS
Y(1)	O(1)	2.307(4)	Y +3.10
	O(2)	2.387(4)	
	O(3)	2.182(6)	
	O(3)	2.187(5)	
	O(4)	2.254(6)	
	O(5)	2.265(5)	
Fe(1)	O(1)	1.879(3)	Fe +2.90
	O(2)	1.867(3)	
	O(4)	1.872(5)	
	O(5)	1.890(4)	

Observed calculated and difference plots from the refinement are shown in Figure 2. Figure 3 shows a representation of the refined structure of Ba_2YFeO_5 comparing the expanded unit cell required to describe this phase, with the smaller cell of Ba_2NdAlO_5. It can be seen that the cell expansion is attributable to the ordered, alternating twisting of the chains of apex-linked YO_6 octahedra which reside in adjacent layers that are stacked up the c-axis (Figure 3b,c).

Structural Characterization of $Ba_3YFe_2O_{7.5}$. X-ray and neutron powder diffraction data collected from $Ba_3YFe_2O_{7.5}$ could be readily indexed using a monoclinic cell [a = 8.0234(1) Å, b = 5.98935(8) Å, c = 18.4565(2), β = 91.225(1)°] with extinction conditions consistent with $P2/c$ spacegroup

dx.doi.org/10.1021/ic3015628 | Inorg. Chem. 2012, 51, 12281−12287

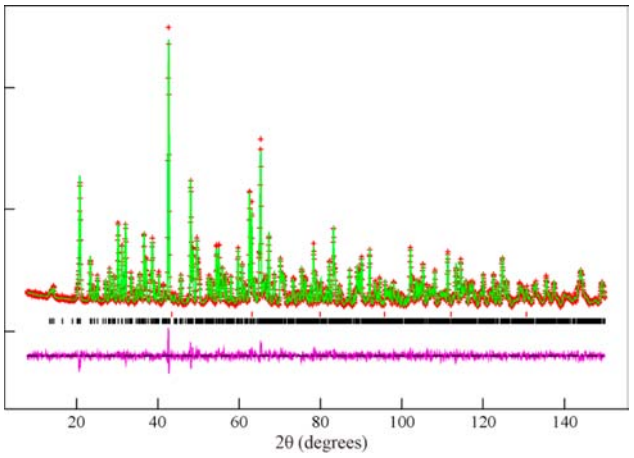

Figure 2. Observed, calculated, and difference plots from the refinement of Ba_2YFeO_5. Lower tick marks indicate peak positions of the title phase; upper tick marks indicate peak positions of the vanadium sample holder.

symmetry. Following the strategy described above, utilized to determine the structure of Ba_2YFeO_5, structural models based on known cation-ordered $Ba_3MM_2'O_{7.5}$ phases were prepared and compared to the diffraction data. A model based on the reported low-temperature, β-phase structure of $Ba_3ErGa_2O_{7.5}$[11] accounted for all of the observed diffraction features well, when erbium was replaced by yttrium and gallium replaced by iron. Therefore, a structural model based on the cation-ordered structure of $Ba_3ErGa_2O_{7.5}$ was refined against neutron powder diffraction data collected from $Ba_3YFe_2O_{7.5}$, and this refinement converged rapidly to yield a good statistical fit (χ^2 = 3.28). Refinement of the yttrium and iron site occupancies revealed no evidence of antisite cation disorder. Full details of the refined structure of $Ba_3YFe_2O_{7.5}$ are given in Table 3, with selected bond lengths in Table 4. Observed calculated and difference plots from the refinement are shown in Figure 4. Representations of the refined structure of $Ba_3YFe_2O_{7.5}$ are shown in Figure 5. Attempts to refine a structural model based on the high-temperature α-phase of $Ba_3ErGa_2O_{7.5}$[11] using a model adapted from the structure of $Sr_3YAl_2O_{7.5}$ recently reported by Wang et al.[12] were unsuccessful as the extinction conditions of the higher space group symmetry of this model ($C2$) could not account for all the diffraction features observed in the data collected from $Ba_3YFe_2O_{7.5}$.

Structural Characterization of $Ba_4YFe_3O_{10}$. X-ray and neutron powder diffraction data collected from $Ba_4YFe_3O_{10}$ could be readily indexed using a primitive cubic unit cell [a = 4.1621(4) Å] consistent with a cation disordered cubic perovskite structure. Refinement of a cation disordered perovskite structural model against neutron powder diffraction data collected from $Ba_4YFe_3O_{10}$ converged rapidly to give a good statistical fit (χ^2 = 2.39). Full details of the refined structure of $Ba_4YFe_3O_{10}$ are given in Table 5. Observed calculated and difference plots from the refinement are shown in Figure 6. As can be seen in Table 5 the oxygen site occupancy refined to a value of 0.821(6) consistent with the phase composition $Ba_4YFe_3O_{10}$ determined by iodometric titration.

Magnetic Characterization. Zero-field cooled and field cooled magnetization data collected from $Ba_nYFe_{n-1}O_{2.5n}$ (n = 2, 3, 4) phases in an applied field of 100 Oe in the temperature range 5 < T/K < 300 are shown in Figure 7. The data collected

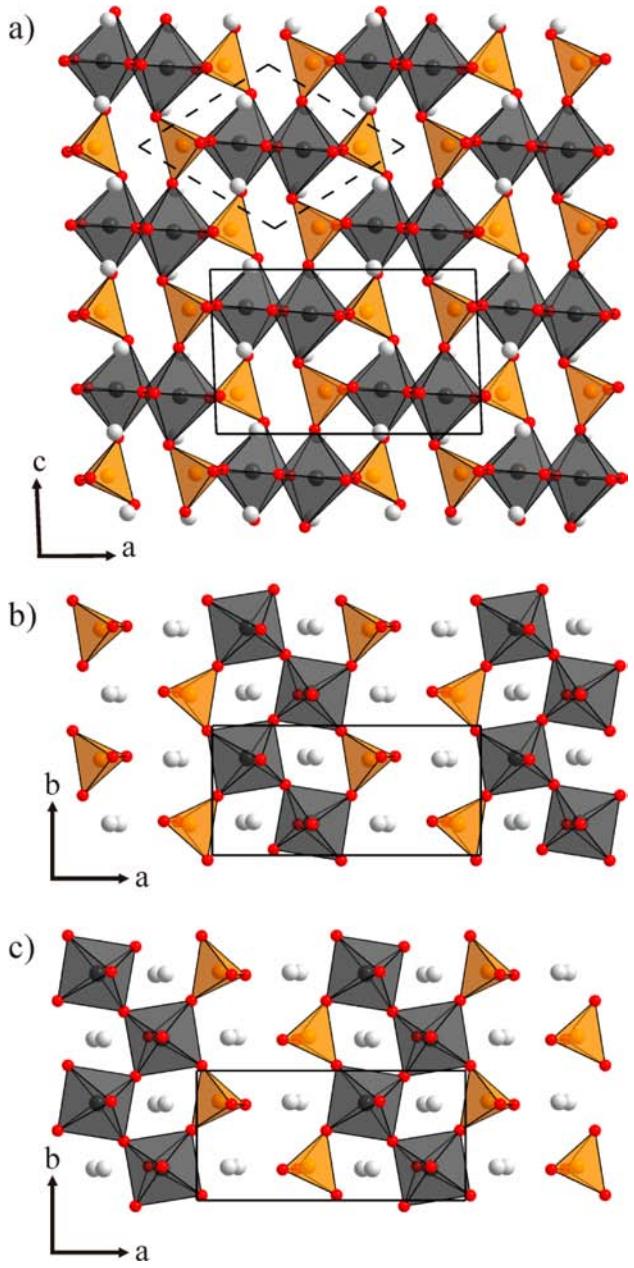

Figure 3. Refined structure of Ba_2YFeO_5. (a) View down the b-axis. Solid line indicates unit cell of Ba_2YFeO_5, broken line indicates the smaller unit cell of Ba_2NdAlO_5. (b) View down the c-axis showing the layer of polyhedra at $z \sim 0.75$. (c) View down the c-axis showing the layer of polyhedra at $z \sim 0.25$.

from Ba_2YFeO_5 and $Ba_3YFe_2O_{7.5}$ can be fitted to the Curie–Weiss law [$\chi = C/(T - \theta)$] over the whole measured temperature range, to yield values of C = 4.84(4) cm^3 K mol^{-1}, θ = −21.5(2) K, and C = 5.05(3) cm^3 K mol^{-1}; θ = −36.6(2) K, respectively. The data collected from $Ba_4YFe_3O_{10}$ can be fitted to the Curie–Weiss law in the temperature range 50 < T/K < 300 to yield values of C = 3.12(3) cm^3 K mol^{-1}, θ = −15.2(2) K. Below 50 K the zero-field cooled and field cooled data diverge weakly, before a large divergence and local maximum in the zero-field cooled data at 20 K, consistent with the onset of magnetic order. Neutron powder diffraction data collected from $Ba_4YFe_3O_{10}$ at 5 K exhibit additional diffraction features compared to the 298 K data (Figure 6) consistent with the onset of magnetic order. These additional diffraction

dx.doi.org/10.1021/ic3015628 | Inorg. Chem. 2012, 51, 12281–12287

Table 3. Refined Structural Parameters of $Ba_3YFe_2O_{7.5}$[a]

atom	site	x	y	z	U_{iso} (Å^2)
Ba(1)	2e	0	0.2824(16)	1/4	0.0057(5)
Ba(2)	2f	1/2	0.3233(13)	1/4	0.0057(5)
Ba(3)	4g	0.0267(5)	0.7529(15)	0.0886(2)	0.0057(5)
Ba(4)	4g	0.4960(7)	0.2505(13)	0.5780(3)	0.0057(5)
Y(1)	4g	0.2453(5)	0.2542(11)	0.4091(1)	0.0044(7)
Fe(1)	4g	0.2464(3)	0.2522(7)	0.0594(1)	0.0020(5)
Fe(2)	4g	0.2293(3)	0.7720(6)	0.2649(1)	0.0046(7)
O(1)	2e	0	0.7983(16)	1/4	0.0190(23)
O(2)	4g	0.0410(5)	0.7647(11)	0.6095(2)	0.0093(4)
O(3)	4g	0.4709(5)	0.2480(13)	0.0892(2)	0.0093(4)
O(4)	4g	0.2744(7)	0.0500(8)	0.3074(2)	0.0093(4)
O(5)	4g	0.2498(7)	0.5548(8)	0.3385(3)	0.0093(4)
O(6)	4g	0.2369(9)	0.4896(9)	0.5002(3)	0.0093(4)
O(7)	4g	0.2299(9)	0.0149(9)	0.9935(3)	0.0093(4)
O(8)	4g	0.3065(7)	0.3365(10)	0.6788(3)	0.0205(14)

[a] $Ba_3YFe_2O_{7.5}$: space group $P2/c$, a = 8.0234(1) Å, b = 5.98935(8) Å, c = 18.4565(2), β = 91.225(1)°, χ^2 = 3.28, wRp = 4.54%, Rp = 3.53%.

Table 4. Selected Bond Lengths from the Refined Structure of $Ba_3YFe_2O_{7.5}$

cation	anion	bond length (Å)	BVS
Y(1)	O(2)	2.318(6)	Y +3.15
	O(3)	2.277(6)	
	O(4)	2.257(6)	
	O(5)	2.223(7)	
	O(6)	2.196(7)	
	O(7)	2.247(7)	
Fe(1)	O(2)	1.910(5)	Fe +2.82
	O(3)	1.872(5)	
	O(6)	1.894(7)	
	O(7)	1.874(6)	
Fe(2)	O(1)	1.861(3)	Fe +3.01
	O(4)	1.873(6)	
	O(5)	1.885(6)	
	O(8)	1.837(6)	

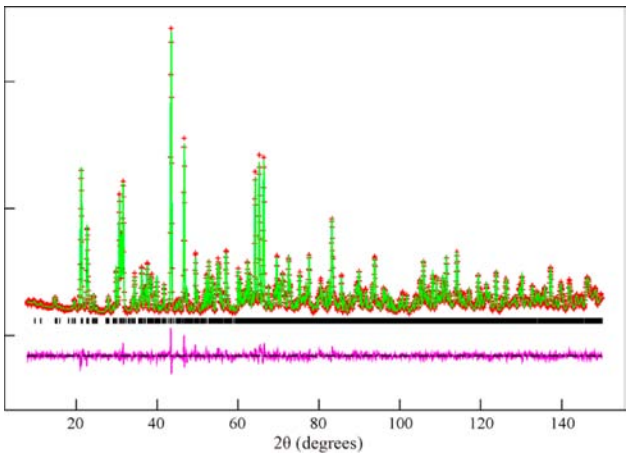

Figure 4. Observed, calculated, and difference plots from the refinement of $Ba_3YFe_2O_{7.5}$. Tick marks indicate peak positions of the title phase.

features were readily indexed using a propagation vector k = ($^1/_2$, $^1/_2$, $^1/_2$), with the intensities of the additional features accounted for by a simple G-type antiferromagnetically ordered

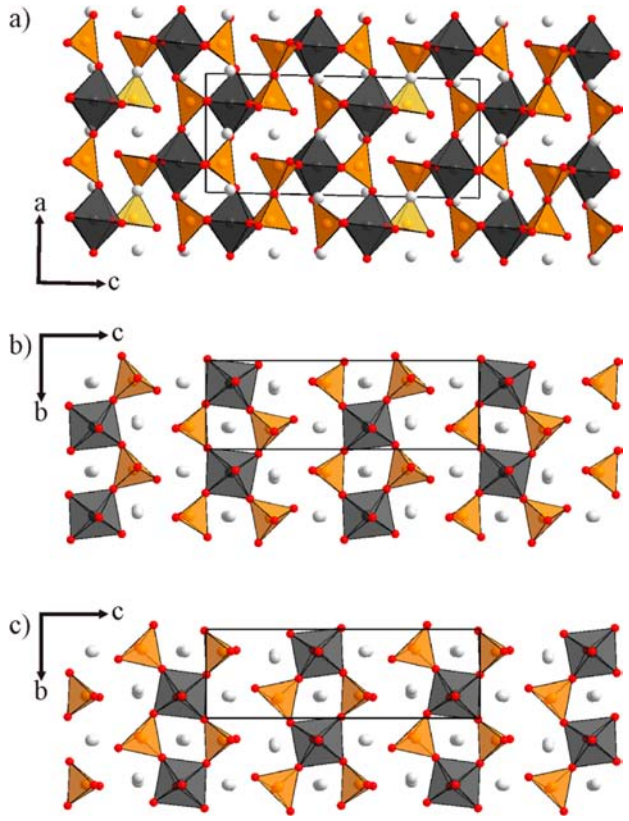

Figure 5. Refined structure of $Ba_3YFe_2O_{7.5}$. (a) View down the b-axis, solid line indicates unit cell. (b) View down the a-axis showing the layer of polyhedra at $x \sim 0.75$. (c) View down the a-axis showing the layer of polyhedra at $x \sim 0.25$.

Table 5. Refined Structural Parameters of $Ba_4YFe_3O_{10}$[a]

atom	site	x	y	z	fraction	U_{iso} (Å^2)
Ba(1)	1b	1/2	1/2	1/2	1	0.002 67(4)
Y/Fe	1a	0	0	0	0.25/0.75	0.005 11(4)
O	3d	1/2	0	0	0.821(6)	0.004 63(4)

[a] $Ba_4YFe_3O_{10}$: space group $Pm\bar{3}m$, a = 4.1624(3) Å, χ^2 = 2.39, wRp = 3.94%, Rp = 5.39%.

arrangement with an ordered moment of 1.78(15) μ_B on each Fe/Y center.

DISCUSSION

The $Ba_nYFe_{n-1}O_{2.5n}$ (n = 2, 3, 4) phases described above can be considered to be variants of the ABO_3 cubic perovskite structure. The n = 2 and n = 3 members of the series adopt cation ordered and anion-vacancy ordered structures with unit cells that are geometric expansions of a simple cubic perovskite cell, $2\sqrt{2} \times \sqrt{2} \times 2$ for Ba_2YFeO_5, $3\sqrt{2} \times \sqrt{2} \times 2$ for $Ba_3YFe_2O_{7.5}$, with 8-fold and 12-fold increases in unit cell volume, respectively, consistent with the cation stoichiometries of the two phases. The n = 4 member of the series adopts a structure with a disordered arrangement of cations and anion-vacancies within a simple unexpended cubic perovskite unit cell.

The n = 2 and n = 3 structures consist of arrays of corner-linked YO_6 octahedra and FeO_4 tetrahedra on the perovskite B-cation sites, with Ba^{2+} cations in large, irregular 9- and 10-coordinate A-sites. The structure of the n = 2 phase Ba_2YFeO_5 is constructed from cation ordered and anion-vacancy ordered $Y_2Fe_2O_{10}\square_2$ subunits which are repeated in a primitive manner

dx.doi.org/10.1021/ic3015628 | Inorg. Chem. 2012, 51, 12281−12287

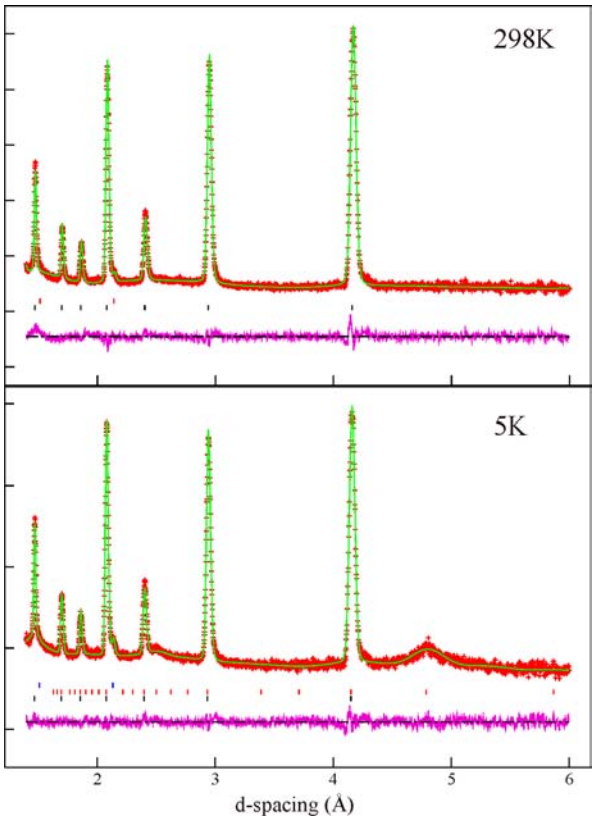

Figure 6. Observed calculated and difference plots from the structural refinement of $Ba_4YFe_3O_{10}$ against neutron powder diffraction data collected at 298 K (top) and 5 K (bottom). Tick marks correspond to peak positions of the title phase and the vanadium sample holder. Additional tick marks in the 5 K data correspond to the magnetic unit cell.

along the *y*- and *z*-axes to form a "slab" in the *yz*-plane, marked green in Figure 8. These $Y_2Fe_2O_{10}\square_2$ slabs are then stacked along the *x*-axis with equivalent slabs, marked in blue in Figure 8, which have been reflected in the *yz*-plane and shifted by *b*/2. The resulting 3D structure of Ba_2YFeO_5 consists of zigzag chains of corner-linked YO_6 octahedra which propagate along the *y*-axis interspersed with FeO_4 tetrahedra, such that there are no Fe−O−Fe linkages anywhere within the lattice.

The structure of $Ba_3YFe_2O_{7.5}$ also contains $Y_2Fe_2O_{10}\square_2$ slabs, marked blue in Figure 8. In this structure, neighboring slabs are related by a $(0, {}^1/_2, {}^1/_2)$ stacking vector and connected by dimers of FeO_4 tetrahedra, marked purple in Figure 8. Thus, the structure of $Ba_3YFe_2O_{7.5}$ can be considered as a composite of Ba_2YFeO_5 and $BaFeO_{2.5}$. Indeed, the dimers of apex-linked FeO_4 tetrahedra observed in the structure of $Ba_3YFe_2O_{7.5}$ are a common structural feature in a number of $BaFeO_{3-x}$ hexagonal perovskite phases.[13,14]

The recurrence of the $Y_2Fe_2O_{10}\square_2$ subunits within the structures of both Ba_2YFeO_5 and $Ba_3YFe_2O_{7.5}$ suggests these blocks can be thought of as secondary building units and constitute a rather stable local configuration. This stability can be rationalized by observing that within each $Y_2Fe_2O_{10}\square_2$ "slab" the yttrium and iron cations adopt a rock-salt-like ordered arrangement. This configuration minimizes the lattice strain within the structure arising from the large difference in the ionic radii of Y^{3+} and Fe^{3+} and also localizes the anion vacancies within the iron coordination polyhedra, maintaining the 6-fold coordination of the yttrium centers. The

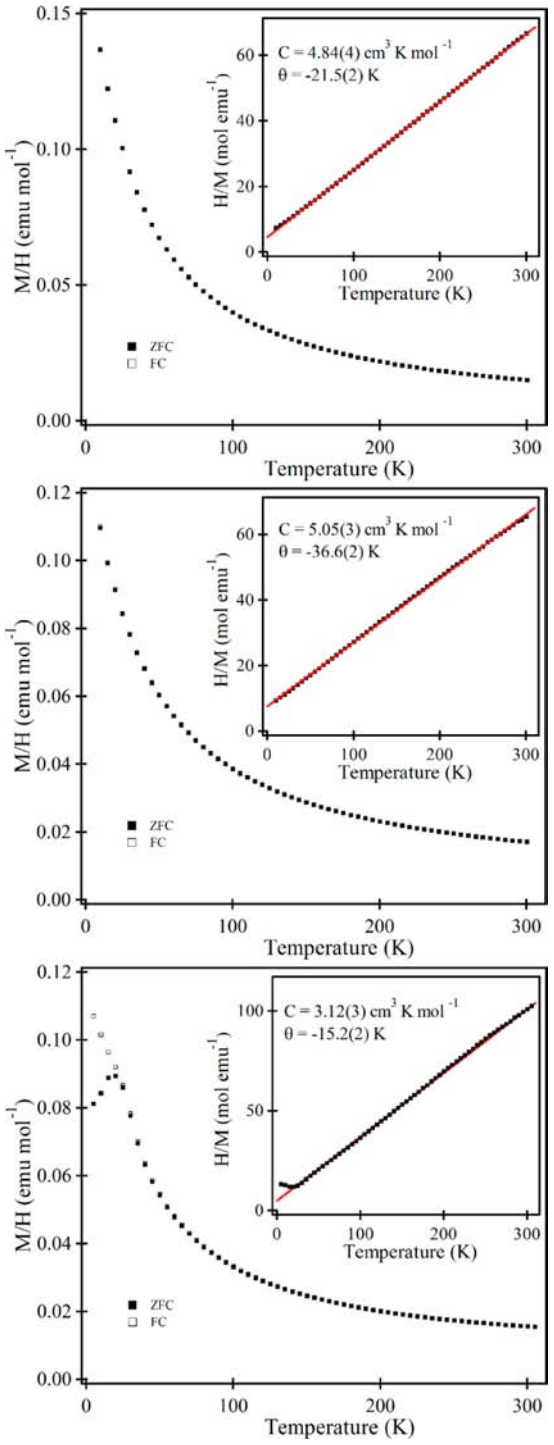

Figure 7. Zero-field cooled and field cooled magnetization data collected from Ba_2YFeO_5 (top), $Ba_3YFe_2O_{7.5}$ (middle), and $Ba_4YFe_3O_{10}$ (bottom). Insets show fits of *H*/*M* to the Curie−Weiss law.

combination of YO_6 octahedra and FeO_4 tetrahedra would be expected to be the most energetically favorable, as the large Y^{3+} cations strongly favor high coordination numbers (≥6) while the smaller d^5 iron cations will tolerate lower coordination numbers and nonoctahedral coordination geometries without significant energetic penalties.

The favorable features of the $Y_2Fe_2O_{10}\square_2$ slabs are retained when they are connected together to form the Ba_2YFeO_5 and

dx.doi.org/10.1021/ic3015628 | *Inorg. Chem.* 2012, 51, 12281−12287

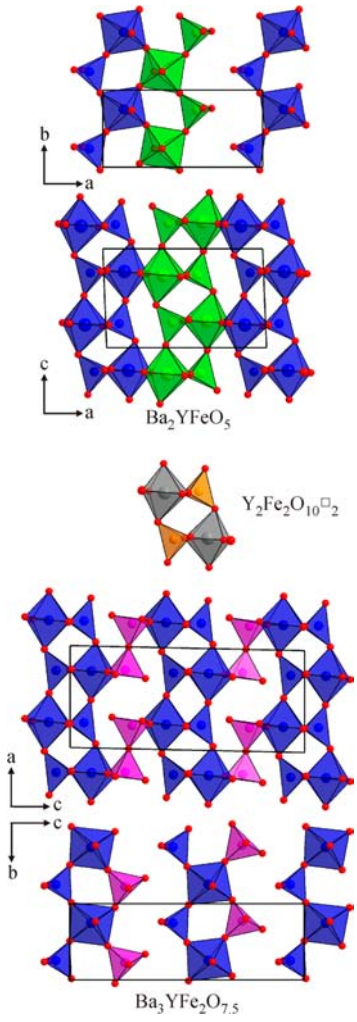

Figure 8. Structures of Ba_2YFeO_5 (top) and $Ba_3YFe_2O_{7.5}$ (bottom) are constructed from $Y_2Fe_2O_{10}\square_2$ cation and anion-vacancy ordered units (middle). In the latter structure these units are combined with apex-linked dimers of FeO_4 tetrahedra.

$Ba_3YFe_2O_{7.5}$ lattices. In the former case the $Y_2Fe_2O_{10}\square_2$ slabs are connected through Y−O−Y linkages which alternate with chains of anion vacancies up the *z*-axis of the interslab interface, so that there are no Fe−O−Fe connections at the interface between slabs, only Y−O−Y links, thus avoiding the lattice strain that would arise from the mismatch between long Y−O and short Fe−O bond lengths. Similarly the linkages between $Y_2Fe_2O_{10}\square_2$ slabs within the $Ba_3YFe_2O_{7.5}$ lattice are made via layers of apex-linked dimers of FeO_4 tetrahedra, such that neighboring slabs are connected via a chain of Y−O−Fe−O−Fe−O−Y bonds. This segregated arrangement of $Y_2Fe_2O_{10}\square_2$ slabs interleaved with sheets of composition $BaFeO_{2.5}$ connects the $Y_2Fe_2O_{10}\square_2$ slabs into a three-dimensional structure while retaining the anion vacancy order of the slabs. This simultaneously maintains the 6-fold and 4-fold coordinations of the Y^{3+} and Fe^{3+} centers while minimizing the lattice strain by having no "competing" Y−O and Fe−O links.

The ordered cation arrangements observed in structures of Ba_2YFeO_5 and $Ba_3YFe_2O_{7.5}$ are unlike those seen previously in transition metal perovskite phases. Typically, double perovskite phases adopt structures with rock salt, columnar, or layered arrangements of B-cations (Figure 1a).[2,3] This is true even when the cation order is being directed by the presence of large numbers of anion vacancies, as is the case for layered $A_2BB'O_5\square$ brownmillerite phases.[6] The unusual cation order observed in the Ba_2YFeO_5 and $Ba_3YFe_2O_{7.5}$ lattices is attributable to the extreme differences in ionic radii of Y^{3+} and Fe^{3+} (Y^{3+} 6CN = 0.90 Å; Fe^{3+} 4CN = 0.49 Å)[15] which would require an extreme cooperative twisting of the B−O−B lattice, if, for example, Ba_2YFeO_5 adopted the brownmillerite structure. Indeed, in all reported brownmillerite phases the B−O bond length of the BO_4 tetrahedral ion is greater than the B′−O bond length of the $B'O_6$ octahedral ion,[16] which is clearly not the case here. Thus, it can be seen that the complex cation order observed in Ba_2YFeO_5 and $Ba_3YFe_2O_{7.5}$ is the result of the differing coordination preferences of the two B-cations and the relative sizes of their ionic radii.

The $n = 4$ member of the $Ba_nYFe_{n-1}O_{2.5n}$ series, $Ba_4YFe_3O_{10}$, adopts a disordered structure in which there is no long-ranged periodicity to the arrangement of the yttrium and iron cations or the anion vacancies within the cubic perovskite lattice. This disordered structure can be attributed to a dilution effect. As noted above the cation ordered and anion vacancy ordered structures of the $n = 2$ and $n = 3$ members of the $Ba_nYFe_{n-1}O_{2.5n}$ series arise to satisfy the coordination preferences of the Y^{3+} and Fe^{3+} cations while minimizing lattice strain. When only $^1/_4$ of the cations are Y^{3+} and only $^1/_6$ of the anion sites are vacant, there are a large number of ways of arranging the cations and anion vacancies on the cubic perovskite lattice which satisfy these criteria, weakening the structure directing effect and leading to a disordered material. It should be noted, however, that a small increase in the concentration of anion vacancies can induce strong cation order in $A_4BB'_3O_{12-x}$ perovskite phases as observed in $Ba_4CaFe_3O_{9.5}$,[8] suggesting that $Ba_4YFe_3O_{10}$ is close to the order/disorder change over point and is thus likely to exhibit cation and anion vacancy order over short length scales.

Magnetism. Magnetization data collected from Ba_2YFeO_5 are consistent with paramagnetic behavior over the measured temperature range ($5 < T/K < 300$) with an observed moment approximately in line with that expected for a spin-only, $s = {}^5/_2$, Fe^{3+} center ($\mu_{expected} = 5.91\ \mu_B$, $\mu_{observed} = 6.22\ \mu_B$).The lack of magnetic order, despite the observation of strong magnetic coupling between Fe^{3+} centers in other phases,[17] is consistent with the absence of an extended Fe−O−Fe lattice in Ba_2YFeO_5.

Magnetization data collected from $Ba_3YFe_2O_{7.5}$ also indicate paramagnetic behavior. However, despite doubling the number of iron centers in each formula unit, the molar susceptibility of $Ba_3YFe_2O_{7.5}$ is only ∼5% larger than that of Ba_2YFeO_5. This suggests that the pairs of iron centers in the dimers of apex-linked FeO_4 tetrahedra are coupled in an antiferromagnetic manner, so they only make a modest contribution to the susceptibility of $Ba_3YFe_2O_{7.5}$, with the majority of the magnetic response coming from the iron centers in the $Y_2Fe_2O_{10}\square_2$ slabs, thus explaining why Ba_2YFeO_5 and $Ba_3YFe_2O_{7.5}$ have very similar magnetic susceptibilities.

$Ba_4YFe_3O_{10}$, in contrast to the $n = 2$ and $n = 3$ members of the $Ba_nYFe_{n-1}O_{2.5n}$ series, exhibits long-range magnetic order at low temperature, consistent with the presence of an extended Fe−O−Fe network in this phase. However the magnetic ordering temperature (50 K) and the size of the ordered moment observed by neutron diffraction (1.78(15) μ_B at 5 K) are both significantly smaller than typically observed for Fe^{3+} cubic perovskite $LnFeO_3$ (Ln = lanthanide) phases,[17] indicating that the presence of Y^{3+} centers in the perovskite B-cation lattice and vacancies in the anion framework significantly

dx.doi.org/10.1021/ic3015628 | *Inorg. Chem.* 2012, 51, 12281−12287

disrupt the magnetic coupling between iron centers in $Ba_4YFe_3O_{10}$.

CONCLUSION

The complex cation order observed in the structures of Ba_2YFeO_5 and $Ba_3YFe_2O_{7.5}$ is attributable to the differing coordination preferences and ionic radii of Y^{3+} and Fe^{3+}. Large YO_6 octahedra and small FeO_4 tetrahedra combine to form $Y_2Fe_2O_{10}\square$ subunits which are then connected into three-dimensional lattices with complex Y/Fe order. Given that neither iron nor yttrium are particularly unusual cations, this suggests that other pairs of cations, which differ from each other in coordination number and size, can also be ordered into novel anion-deficient cation-ordered frameworks if their local coordination preferences are sufficiently robust. Furthermore, the observation of $Y_2Fe_2O_{10}\square_2$ secondary building units within the ordered lattices of Ba_2YFeO_5 and $Ba_3YFe_2O_{7.5}$ provides a basis of understanding the interactions that direct the aggregation and ordering of the cations in such phases, allowing the choice of cation pair and sample stoichiometry to be guided, and an element of design added, to the process of preparing new cation ordered phases.

AUTHOR INFORMATION

Corresponding Author

*E-mail: michael.hayward@chem.ox.ac.uk. Phone: +44 1865 272623. Fax: +44 1865 272690.

Author Contributions

The manuscript was written through contributions of all authors. All authors have given approval to the final version of the manuscript.

Notes

The authors declare no competing financial interest.

ACKNOWLEDGMENTS

We thank E. Suard and R. Smith for assistance collecting the neutron powder diffraction data. Experiments at the ISIS pulsed neutron facility were supported by a beam time allocation from the Science and Technology Facilities Council. K.L. thanks the Pacific Alliance Group for a scholarship.

REFERENCES

(1) Cooper, S. L.; Egami, T.; Goodenough, J. B.; Zhou, J.-S. *Localized to Itinerant Electronic Transition in Perovskite Oxides*; Springer-Velang: Berlin, 2001.
(2) King, G.; Woodward, P. M. *J. Mater. Chem.* **2010**, *20*, 5785.
(3) Anderson, M. T.; Greenwood, K. B.; Taylor, G. A.; Poeppelmeier, K. R. *Prog. Solid State Chem.* **1993**, *22*, 197.
(4) Meneghini, C.; Sugata, R.; Liscio, F.; Bardelli, F.; Mobilio, S.; Sarma, D. D. *Phys. Rev. Lett.* **2009**, *103*, 46403.
(5) Millange, F.; Caignaert, V.; Domenges, B.; Raveau, B.; Suard, E. *Chem. Mater.* **1998**, *10*, 1974.
(6) Antipov, E. V.; Abakumov, A. M.; Istomin, S. Y. *Inorg. Chem.* **2008**, *47*, 8543.
(7) Tenailleau, C.; Allix, M.; Claridge, J. B.; Hervieu, M.; Thomas, M. F.; Hirst, J. P.; Rosseinsky, M. J. *J. Am. Chem. Soc.* **2008**, *130*, 7570.
(8) Turp, S. A.; Hargreaves, J.; Baek, J.; Halasyamani, P.; Hayward, M. A. *Chem. Mater.* **2010**, *22*, 5580.
(9) Larson, A. C.; Von Dreele, R. B. *Los Alamos Natl. Lab., [Rep.] LA (U. S.)* **2000**, 86−748.
(10) Antipov, E. V.; Lykova, L. N.; Korba, L. M. *Koord. Khim.* **1985**, *11*, 1151.
(11) Abakumov, A. M.; Shpanchenko, R. V.; Lebedev, O. I.; Van Tendeloo, G.; Amelinckx, S.; Antipov, E. V. *Acta Crystallogr., Sect. A* **1999**, *55*, 828.
(12) Wang, C.-H.; Guo, D.-F.; Li, Z.-F.; Wang, X.-M.; Lin, J.-H.; Zeng, Z.-Z.; Jing, X.-P. *J. Solid State Chem.* **2012**, in press.
(13) de Muro, I. G.; Insausti, M.; Lezama, L.; Rojo, T. *J. Solid State Chem.* **2005**, *178*, 1712.
(14) Delattre, J. L.; Stacy, A. M.; Slegrist, T. *J. Solid State Chem.* **2004**, *177*, 928.
(15) Shannon, R. D. *Acta Crystallogr.* **1976**, *A32*, 751.
(16) Parsons, T. G.; D'Hondt, H.; Hadermann, J.; Hayward, M. A. *Chem. Mater.* **2009**, *21*, 5527.
(17) Goodenough, J. B.; Longo, J. M. *Landolt-Börnstein Tabellen*; Springer: Berlin, 1970.